Effect of Zeolitic Imidazolate Framework Topology on the Purification of Hydrogen from Coke Oven Gas

Please check the document version of this publication:

• A submitted manuscript is the version of the article upon submission and before peer-review. There can be important differences between the submitted version and the official published version of record. People interested in the research are advised to contact the author for the final version of the publication, or visit the DOI to the publisher's website.
• The final author version and the galley proof are versions of the publication after peer review.
• The final published version features the final layout of the paper including the volume, issue and page numbers.

Link to publication

Download date: 04. Oct. 2023

Research Article

Effect of Zeolitic Imidazolate Framework Topology on the Purification of Hydrogen from Coke Oven Gas

Xiucheng Huang, Ana Martín-Calvo,* Martijn J. J. Mulder, Sjoerd C. J. van Acht, Juan José Gutiérrez-Sevillano, Julio C. García-Navarro, and Sofía Calero*

Cite This: ACS Sustainable Chem. Eng. 2023, 11, 8020−8034
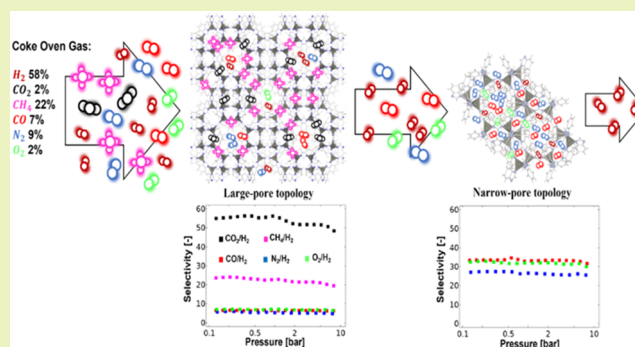
Read Online

ACCESS | Metrics & More | Article Recommendations | Supporting Information

ABSTRACT: This work aims to shed light on the performance of zeolitic imidazolate frameworks for hydrogen purification from coke oven gases (COG). Using molecular simulation, we model COG as a mixture of six gases and study the effect of ZIF topology on the separation performance. To do this, we compare similar structures, *e.g.*, ZIF-8 and ZIF-11, and focus on obtaining information that explains why they behave differently while being so similar. Simulation results show that the structure with the smallest pore size best separates hydrogen from carbon monoxide and nonpolar molecules. The adsorption of carbon dioxide is also strongly affected by the polarizability of the structure. However, the adsorption of the other components (methane, carbon monoxide, nitrogen, and oxygen) is strongly dependent on their pore size. We also provide molecular information on the effect of phase transition on hydrogen purification using ZIF-7 as an example, which drastically changes the pore volume of the structure when it changes phase. These findings will help to select high-performance ZIFs for adsorption- or screening-based hydrogen purification.

KEYWORDS: hydrogen separation, coke oven gas, adsorption selectivity, ZIFs, topology, GCMC simulation

INTRODUCTION

Hydrogen is one of the most promising renewable energy carriers. Approximately 95% of current hydrogen production utilizes the method of steam methane reforming (SMR) by consuming natural gas (NG), producing a syngas mixture containing 70−80% of hydrogen.[1,2] There are several other ways of hydrogen production. Great efforts have been made to produce hydrogen from alternatives, including water electrolysis by proton electrolyte membrane[3] and biomass through biological or thermochemical methods.[4] A significant amount of hydrogen is also present in coke oven gas (COG).[5] Steel production utilizes coke as a reducing agent and yields a byproduct of the hydrogen-rich COG stream.[6] In China, 70 billion Nm³ COG was produced annually for furnace heating purposes due to its typical calorific value (CV) of 19.9 MJ Nm⁻³, and approximately 80% of the volume was disposed to the atmosphere without an effective recovery.[7] Hence, there is a potential market for utilizing COG from the waste stream of steel manufacture as a hydrogen source to meet the growing worldwide demand for low-carbon hydrogen.[8] Both syngas (from SMR production) and COG contain significant amounts of methane, carbon dioxide, and carbon monoxide.[5] Impurities (*e.g.*, nitrogen, oxygen) or other trace components may still be present after the pretreatment of COG.[6] Fuel cell electric vehicles have received significant attention over the past

decade due to the increasing number of vehicles deployed worldwide. Polymer electrolyte membrane fuel cells (PEMFC) are one of the most emerging technologies due to their fast start-up, high power−weight ratio, and low operation temperature (<80 °C).[1] However, the platinum electrocatalysts used in PEMFC are sensitive even to trace levels of certain impurities, such as carbon monoxide.[9] Carbon dioxide may also indirectly affect the fuel cell by reacting on the catalyst and forming carbon monoxide (reaction commonly known as reverse water−gas shift, or RWGS).[3,10] For these reasons, the fuel quality standard ISO 14687:2019 for PEMFC vehicles states that the CO_2 content in the hydrogen should not exceed 2 ppm and CO should not exceed 0.2 ppm.[11]

The production of high-quality H_2 with the desired low contaminant levels is achievable with existing purification processes. The commercial technology widely used for hydrogen purification and separation from SMR is pressure swing adsorption (PSA).[12] Porous solid adsorbents like

zeolites and activated carbons are widely used in PSA processes.[13−15] A critical stage in the realization of the hydrogen economy is the production of commercially cheap hydrogen.[11] A considerable amount of penalties would incur to PSA in terms of energy efficiency. Traditional PSA materials can exhibit poor selectivity and require energy-intensive regeneration, which induces low productivity (consequently a high percentage of hydrogen losses) and high energetic costs.[12,16] It has also been found that zeolites and activated carbons preferentially adsorb CO_2, partially inhibiting CO removal.[1,5,17] Several studies have focused on the optimization of PSA performance using CuCl-modified adsorbents to enhance CO adsorption affinity, thus increasing its selectivity.[1,5,6,18] The main issue is the need for a vacuum pressure to desorb carbon monoxide from the copper metal center. This desorption swing increases the capital costs of the PSA unit and the operation complexity due to a stronger interaction of CO with CuCl adsorbents than zeolites and activated carbons.[19]

Metal−organic frameworks (MOFs) are a family of hybrid porous materials formed by the coordination of metal ions with organic linkers, resulting in a highly porous structure.[20] MOFs represent an excellent alternative (good selectivity and tunability)[19] to conventional materials like zeolites and activated carbons.[12] To date, a large number of different MOFs have been synthesized, which have shown various promising applications in gas storage and separation.[12,20−22] As a subclass of MOFs, zeolitic imidazolate frameworks (ZIFs) have drawn more and more attention nowadays.[20] ZIFs are porous crystalline materials with tetrahedral networks resembling zeolites with transition metals (Zn, Co) linked by imidazolate ligands.[20] The well-defined pore sizes in conjunction with a high surface area make ZIFs prime candidates for molecular sieving.[23] ZIFs can be either grown in dense layers to form pure inorganic membranes on porous supports or dispersed within a polymer phase to form mixed matrix membranes.[24−28] Among the many ZIFs synthesized, some of them have exceptional thermal and chemical stability and exhibit great promise for hydrogen separation and purification.[20,23]

ZIF-7 is one of the earliest reported and most promising ZIFs for applications involving CO_2 separation from flue gas and natural gas sources.[29] ZIF-8 is the most widely studied ZIF for industrial applications, such as natural gas purification and CO_2 capture from flue gas.[23,30] For hydrogen production and purification technology, ZIF-11 has been identified as the most promising candidate for membrane-based hydrogen separation.[23] Thornton et al.[23] have remarked on the great H_2-sieving capabilities of ZIF-11 that could significantly revolutionize the hydrogen production industry if incorporated within a suitable polymer base configuration that maximizes gas-to-ZIF contact. Almost all studies in ZIFs have been carried out on either pure components or binary mixtures, although a few cases focusing on the ternary mixture separation can be found in the literature.[31] There is a need to study ZIF separation performances with multicomponents, including carbon monoxide, the most detrimental electrocatalyst poison in these gas mixtures. To the best of our knowledge, CO adsorption behavior in ZIFs has only been investigated experimentally in ZIFs at cryogenic temperatures.[32−34] There is still a lack of insight into CO adsorption behavior in ZIFs.

Various zeolitic topologies have been reported in ZIFs by employing different imidazolate ligands.[35] The same topology

can have different metal ions and ligands. The synthetic control also allows frameworks to have the same chemical compositions but different topologies. The topological diversity puts forward a challenge for experimental screening aimed at a specific purpose in adsorption.[36] With this in mind, simulation tools such as the Grand Canonical Monte Carlo (GCMC)[37] can offer an advantage over experiments to predict the adsorption behaviors for various adsorbates in MOFs, leading to the clarification of structure−property relationships. Many groups reported their studies on various ZIFs using GCMC simulation, indicating that adsorption behavior and selectivity are strongly affected by ZIF topology. Morris et al.[38] have investigated the role of topologies in the adsorption of carbon dioxide at low and high pressures in a combined experimental−computational approach. They show that the topologies with the smaller pores have larger adsorption than their large-pore counterparts at low pressures. The reverse occurs at high pressures, where the larger-pore topologies have significantly higher adsorption. This phenomenon was also observed by Gao et al.[39] for water adsorption in various ZIFs with RHO and SOD topologies. In the study of adsorption and separation of ethane/ethylene in ZIF-8, Wu et al.[36] suggested that adsorption behaviors are strongly affected by ZIF topology rather than the organic linker. Han et al.[40] studied the hydrogen uptake behavior of six different ZIF topologies, suggesting that H_2 adsorption sites are strongly correlated to topologies and that the saturation capacity depends significantly on their surface area and pore size.

In this work, we are developing a new set of force-field parameters that are validated by comparing simulated results with experimental data. The adsorption of pure- and multicomponent gases is investigated with GCMC simulation using the new force field and RASPA code.[41] Adsorption isotherms, isosteric heats of adsorption, average occupation profiles, radial distribution functions, and adsorption selectivity are obtained to give insight into the topological effect on COG adsorption behaviors and hydrogen purification performances in various ZIFs.

■ COMPUTATIONAL DETAILS

Using molecular simulation as a predictive tool requires reliable and effective force fields able to predict interactions between frameworks and adsorbates. van der Waals interactions of guest−guest and host−guest are described with 12-6 Lennard-Jones (LJ) potential in conjunction with Coulombic potential.[42] The cross-interaction parameters are approximated by the Lorentz−Berthelot mixing rules.[43] Lennard-Jones potentials are cut and shifted with a cutoff distance of 12 Å. Coulombic interactions are computed with the Ewald summation method with a relative precision of 10^{-6}. To obtain the number of adsorbed molecules in ZIFs, Monte Carlo simulations are performed using the RASPA code with the grand canonical ensemble where chemical potential, volume, and temperature are kept fixed.[41] The numbers of unit cells of frameworks adopted in this simulation are $2 \times 2 \times 2$, and periodic boundary conditions are applied in all three dimensions. The frameworks are treated as rigid during simulation. Fugacity is obtained from the chemical potential, and it is directly related to pressure by the fugacity coefficient, using the Peng−Robinson equation of state.[44] A total of 1×10^7 steps are used; the first half of these moves is used for equilibration, and the remaining steps are used for calculating the ensemble averages. We used translation, random insertion,

and deletion moves for pure-component simulations. An additional move named identity swap is included for multicomponents to accelerate the convergence and reduce statistical errors. Every possible move is given an equal probability.[45] Compared to experimental data, simulated absolute adsorption loading is converted to excess adsorption.[46]

Carbon dioxide is modeled as a rigid linear molecule. This model has three LJ sites centered at each atom. The parameters for carbon and oxygen atoms are listed in Table 1. The intrinsic quadrupole moment is described by a partial

Table 1. Lennard-Jones Parameters, Point Charges, and Bond Lengths for the Models of Carbon Dioxide, Carbon Monoxide, Nitrogen, Oxygen, Methane, and Hydrogen[49−52,66]

adsorbate molecules			
atoms	ε/k_B (K)	σ (Å)	charges (e^-)
C (CO_2)	29.933	2.744	0.6512
O (CO_2)	85.671	3.017	−0.3256
C (CO)	16.141	3.658	−0.2424
O (CO)	98.014	2.979	−0.2744
dummy (CO)			0.5168
O (O_2)	53.023	3.045	−0.112
dummy (O_2)			0.224
N (N_2)	38.298	3.306	−0.405
dummy (N_2)			0.810
CH_4	158.5	3.72	0
H_2	36.733	2.958	0
bond	distance (Å)		
C-O (CO)	1.128		
C-dummy (CO)	0.6443		
N-N (N_2)	1.1		
N-dummy (N_2)	0.55		
O-O (O_2)	1.208		
O-dummy (O_2)	0.604		
C-O (CO_2)	1.16		

charge model with point charges placed at each site. Details about the use of this type of model in ZIFs can be extensively found in the literature.[47−49] Methane is modeled as a single-center LJ molecule, with no charges considered.[50] Nitrogen, oxygen, and carbon monoxide are presented based on a three-site model with LJ parameters, point charges in all of their atoms, and charged dummy atoms without mass to reproduce the polarity of the molecules.[51] Many groups reported their models for simulating hydrogen and its interactions with porous materials. Deeg et al.[52] and van den Berg et al.[53] treated hydrogen as a single noncharged LJ center, while Pantatosaki and Papadopoulos simulated hydrogen as an LJ center bearing a quadrupole moment.[54] It has been shown that the effect of electrostatic interactions for hydrogen adsorption was essentially negligible at room temperature due to a weak quadrupole moment.[55] Therefore, a single spherical LJ center noncharged is used in this work to describe hydrogen's interactions. In Table 2, dipole and quadrupole moments for each component are computed from the simulation and compared with molecule polarizability from the reference.

Due to their nature, the topology of ZIFs relates to that of zeolites as reported in the Database of Zeolite Structures. Each topology is assigned as a three-capital-letter code in alphabetical order (*e.g.*, SOD, RHO, GME, and DFT) that describes

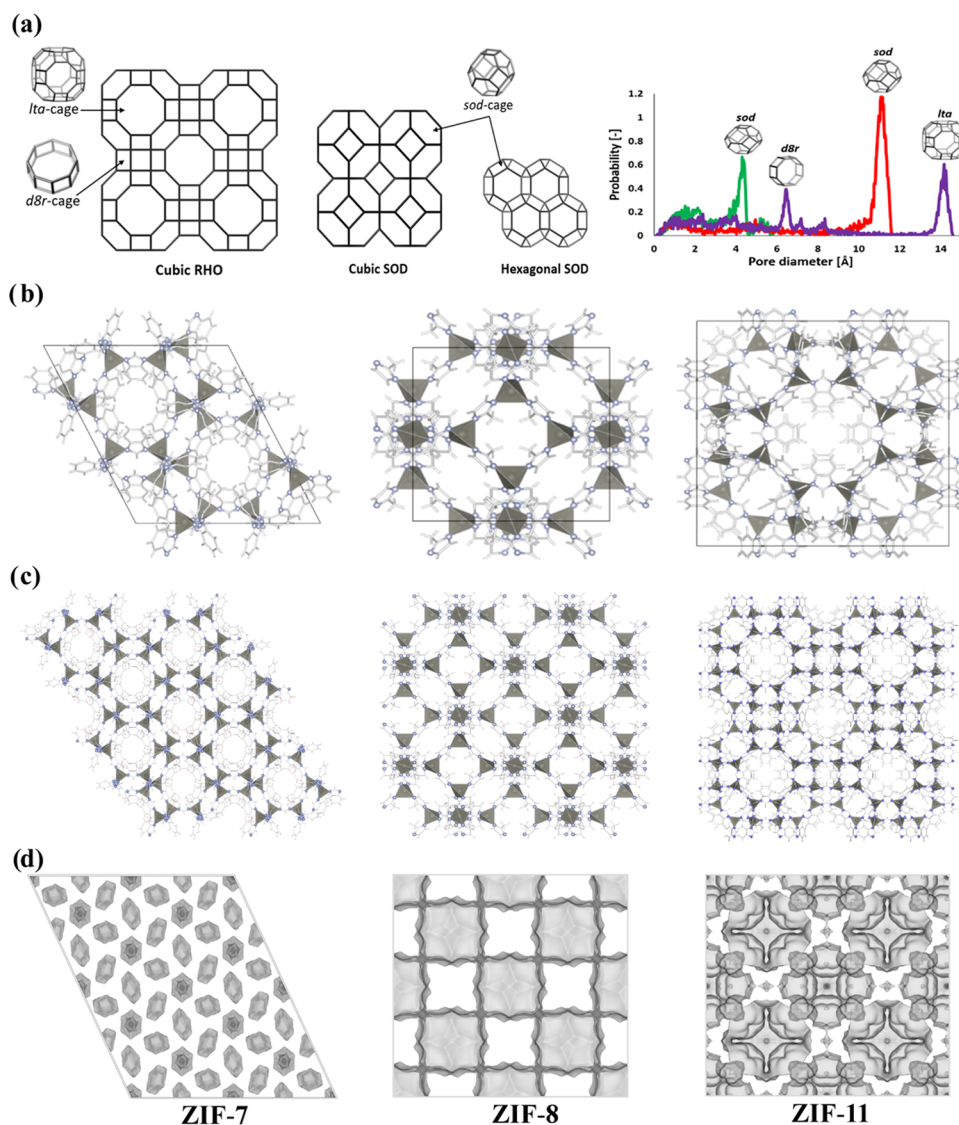**Table 2. Electronic Properties of the Adsorbate Gases in This Work**

molecules	polarizability[b] (Å)	dipole moment[a] (D)	quadrupole moment[a] (D Å)
CO_2	2.91	0	4.21
CH_4	2.59	0	0
CO	1.95	0.11	0.79
N_2	1.74	0	1.18
O_2	1.58	0	0.39
H_2	0.80	0	0

[a]Calculated by RASPA code. [b]Kim et al.[71] and Rallapalli et al.[72]

the network of tetrahedrally coordinated framework atoms and symmetry of the unit cell,[56−58] as implemented by the International Zeolite Association (IZA). On the one hand, the same topology with different ligands can have different pore sizes, surface areas, and symmetry shapes. For instance, ZIF-8 and ZIF-7 have the same type of topology with tetrahedral Zn(II) linked by different ligands:[59] methylimidazolate (mIM) and benzimidazole (bIM), respectively. The unit cell of both ZIF-8 and ZIF-7 contains six four-membered rings and eight six-membered rings $[4^6 \times 6^8]$, which corresponds to the SOD zeolite-type topology composed of *sod*-cages.[43,60] ZIF-8 crystallizes in a cubic symmetry forming pore cages connected by six-membered rings, but the ligand of ZIF-7 facilitates the crystallization in rhombohedral symmetry with hexagonal cages.[60] ZIF-7 topology also features framework flexibility. This feature could induce a narrow-to-large pore phase transition that significantly affects adsorption and separation behaviors.[29] On the other hand, chemically identical ZIFs can have different topologies. ZIF-7 and ZIF-11, for example, possess the same metal ion Zn(II) and the same organic unit benzimidazolate, but different topologies.[61,62] Compared to ZIF-7, the cubic unit cell of ZIF-11 is composed of four, six, and eight-membered rings $[4^{12} \times 6^8 \times 8^6]$, which refers to the RHO topology.[62] This topology consists of *d8r*- and *lta*-cages.[38,58,61] ZIF-7 topology gives the accessible surface area (887 m²/g) and has a prominent pore size of 4.31 Å. The pore size distribution (PSD) is calculated with the RASPA code by using the Gelb and Gubbins' method.[63,64] The topological structure of ZIF-11 results in a larger accessible surface area (1694 m²/g), and the PSD indicates two peaks at 6.22 Å (*d8r*-cage) and 14.17 Å (*lta*-cage). ZIF-8 has the same type of topology as ZIF-7 but yields a large surface area (1990 m²/g) and pore size of 11.07 Å. The topological visualization and structural properties for ZIF-7, -8, and -11 are summarized in Figure 1 and Table 3. In the case of purely ionic material, charges of the Zn cations are equal to their formal charges, *i.e.*, +2e. In this work, Zn charges are employed to be smaller than the formal ones due to the covalent interaction of the chemical bonds in the frameworks. The reduction of the charges is normally employed, and the cations vary typically between +0.3e and +1.7e. The new sets of atomic charges for ZIF-7, ZIF-8, and ZIF-11 are shown in Figure S1.

Generic force fields such as Universal Force Field (UFF)[65] have the advantage of being easy to implement for modeling any of ZIFs based on Zn/Co with various imidazolate molecules, but they tend to overestimate the experiment.[20,66] Since adsorption isotherms are sensitive to Lennard-Jones parameters, UFF Lennard-Jones parameters are optimized by fitting to experimental measurements. This fitting method has also been applied for obtaining new sets of transferable force

Figure 1. Structure and topology of ZIFs in this work. (a) Topologies and PSD (calculated from RASPA code) for ZIF-7 (green), ZIF-8 (red), and ZIF-11 (purple). (b) Unit cells. (c) 2 × 2 × 2 cells for GCMC simulation. (d) Pore shape and connectivity. ZIF-7 features disconnected cages in a hexagonal shape. Cubic cages in ZIF-8 are connected by six-membered rings. The fusion of ZIF-11 cages is through 4-rings, 6-rings, and double 8-ring window channels.

Table 3. Structural Properties of ZIFs Studied in This Work

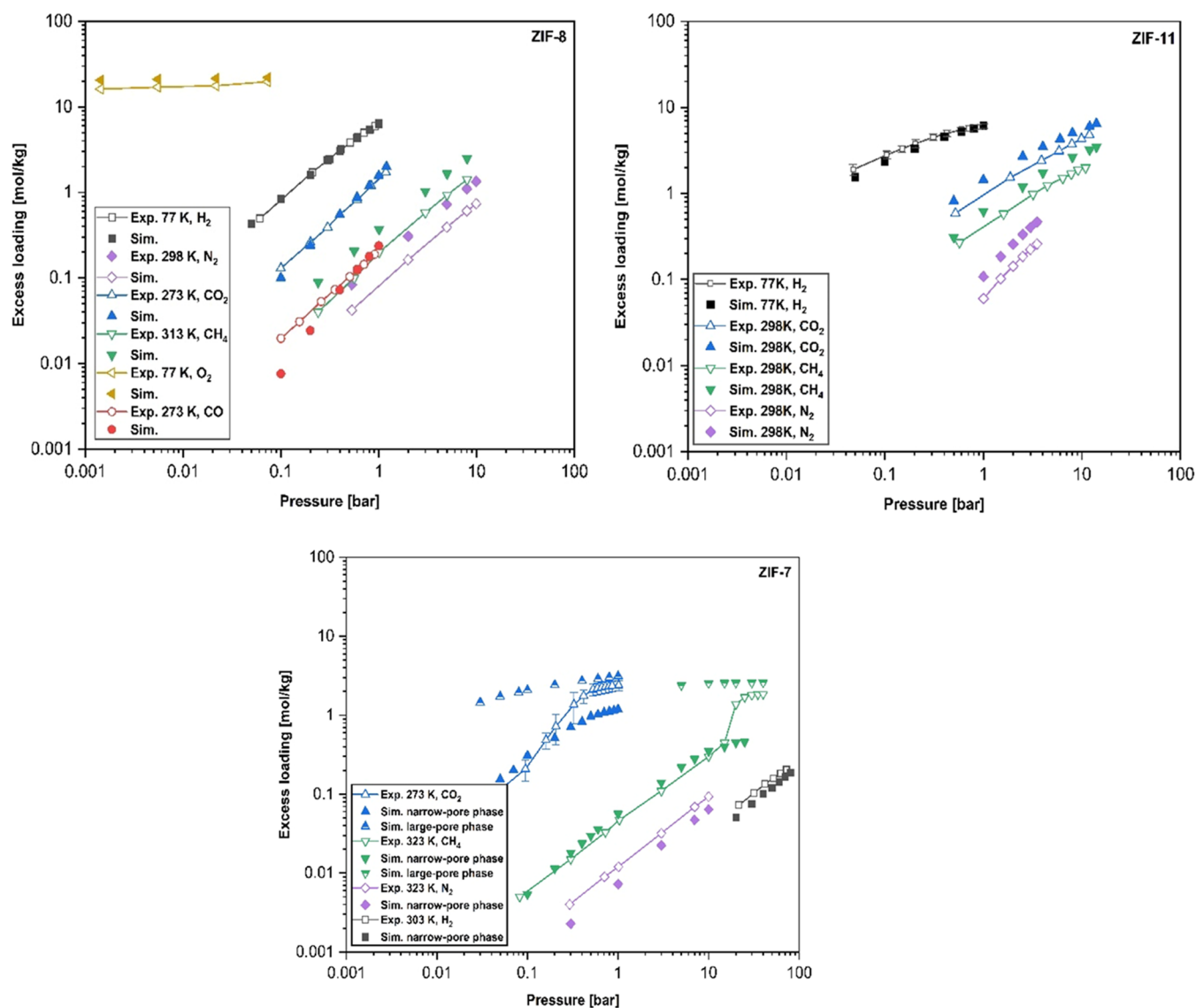| ZIF[b]	composition	topology	density[a] (cm^3/g)	pore aperture diameter[b] (Å)	surface area[a] (m^2/g)	accessible pore volume (cm^3/g)
ZIF-7_narrow[c]	Zn(bIM)2	SOD	1.384	2.9	34.72	0.02
ZIF-7_large[b]	Zn(bIM)2	SOD	0.806	2.9	886.82	0.22
ZIF-8	Zn(mIM)2	SOD	1.082	3.4	1989.72	0.54
ZIF-11	Zn(bIM)2	RHO	0.996	3.0	1693.61	0.41

[a]Calculated by RASPA code. The surface area is probed using nitrogen. [b]Obtained from Park et al.[35] [c]Obtained from Klein et al.[73] The full synthetic procedures for ZIF-7, ZIF-8, and ZIF-11 can be found in the Supporting Information of their work.

fields for gas adsorption in Zeolite by García-Sánchez et al.[49] and Martin-Calvo et al.[51] The adsorption of carbon dioxide in ZIF-8 is particularly selected for the refinement to obtain a new set of Lennard-Jones parameters (Table 4). One of the reasons for this choice is that ZIF-8 is a well-synthesized material with a high degree of crystal purity.[67] Another factor is associated with the structural phase transition. Although the structural flexibility of ZIF-8 plays a vital role in the diffusion[68] and adsorption[32] of guest molecules, many studies indicated that ZIF-8 is a structural-stable framework with good rigidity.

Table 4. Lennard-Jones Force-Field Parameters for ZIFs

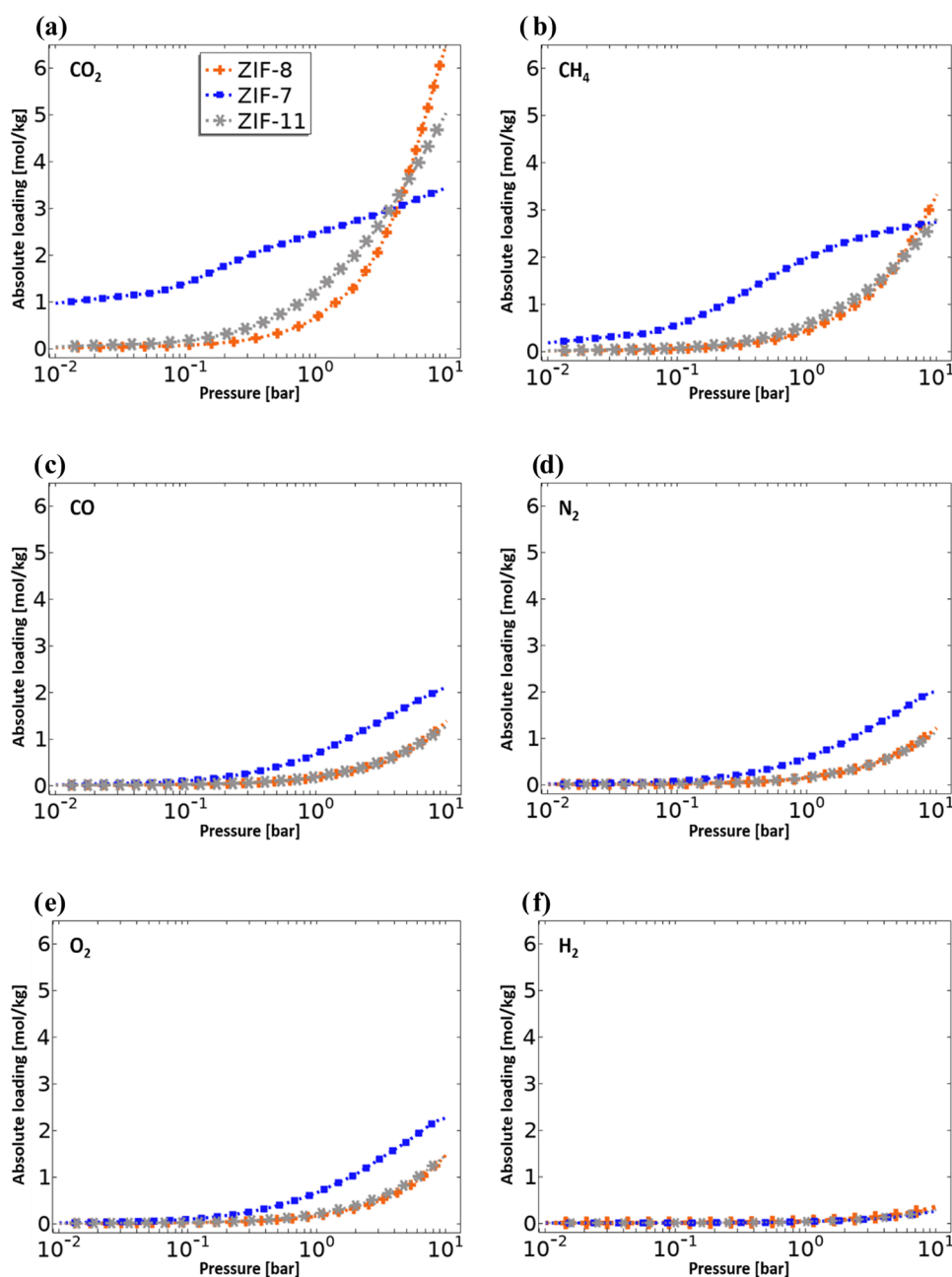| atoms	universal force field[a]		this work	
	ε/k_B (K)	σ (Å)	ε/k_B (K)	σ (Å)
Zn	62.4	2.46	62.4	2.24
C	52.84	3.43	52.84	3.12
N	34.72	3.26	34.72	2.97
H	22.14	2.57	22.14	2.34

[a]Obtained from Rappe et al.[65]

Figure 2. Comparison between the experimental (open) and calculated (closed) adsorption isotherms of CO (red), CO_2 (blue), CH_4 (green), N_2 (purple), O_2 (yellow), and H_2 (black) in ZIF-7, ZIF-8, and ZIF-11. Experimental data for ZIF-8: H_2 (77 K),[35,76] CO_2 (273 K),[66,77] CH_4 (313 K),[78] N_2 (298 K),[78] O_2 (77 K),[32] and CO (273 K).[79] Experimental data for ZIF-11: H_2 (77 K),[23,35,62] CO_2 (298 K),[80] N_2 (298 K),[81] and CH_4 (298 K).[80] Experimental data for ZIF-7: H_2 (303 K),[73] N_2 (323 K),[29] CO_2 (273 K),[29,60,74,82] and CH_4 (323 K).[29] Since experimental CO_2 data on ZIF-7 are taken from multiple sources, we plot the average value with standard deviation.

Pantatosaki et al.[69] reported that the framework flexibility has no significant influence on CH_4 and CO_2 adsorption up to 100 bar in ZIF-8 at 300 K. Zhang et al.[70] simulated adsorption isotherms (<100 bar, 298 K) of CH_4 and CO_2 from rigid and flexible models, where no structural transition was observed in ZIF-8. The kinetic diameter of CO_2 (3.3 Å)[52] is smaller than the aperture size of the structure of ZIF-8 (3.4 Å), which makes the adsorption less affected by kinetic impediments.[51] More information about the fitting to experimental data can be found in the Supporting Information (Figures S2 and S3).

RESULTS AND DISCUSSION

Force-Field Validation. To ensure the transferability of the new force field parameters, adsorption isotherms of carbon dioxide, methane, carbon monoxide, nitrogen, and hydrogen over ZIF-7, ZIF-8, and ZIF-11 are computed and compared to experimental data at different temperatures. The calculated results shown in Figure 2 for ZIF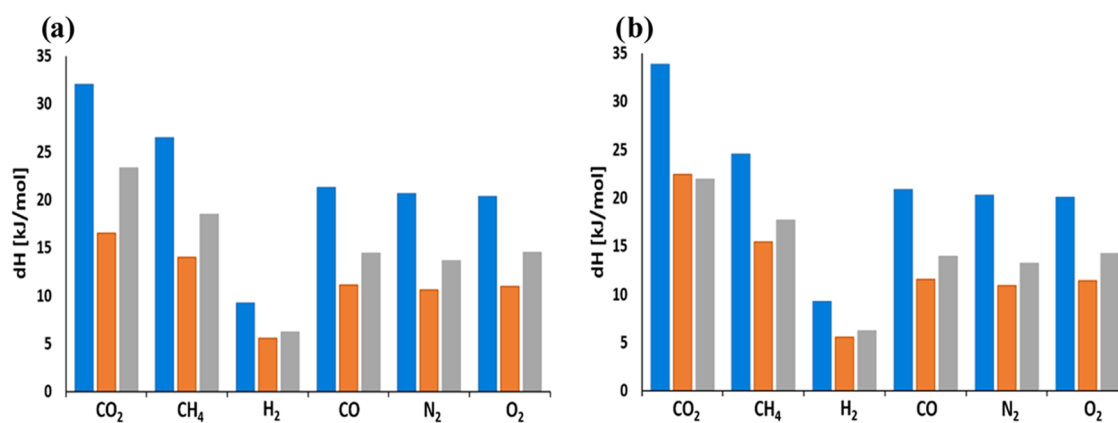-8 and ZIF-11 are generally in agreement with experimental data for all of the gases at either cryogenic or room temperature, regardless of the two frameworks having different topological structures composed of different ligands. The new force field exhibits excellent prediction for the adsorption isotherms of carbon dioxide and hydrogen in ZIF-8 and ZIF-11. Small differences are observed for N_2 and CH_4 adsorption. In both cases, experimental and calculated isotherms follow the same trend, but simulation data slightly overestimate experimental values. This is a common deviation normally attributed to the presence of small impurities in the experimental material that reduces the accessible volume of the structure. This effect is not observed in the simulation results as the structures are completely crystalline and free of impurities and defects. In a similar way, the presence of impurities acts as additional adsorption sites for polar molecules, such as CO, explaining the smaller adsorption compared to the experimental values found for CO in ZIF-8 up to 0.3 bar.
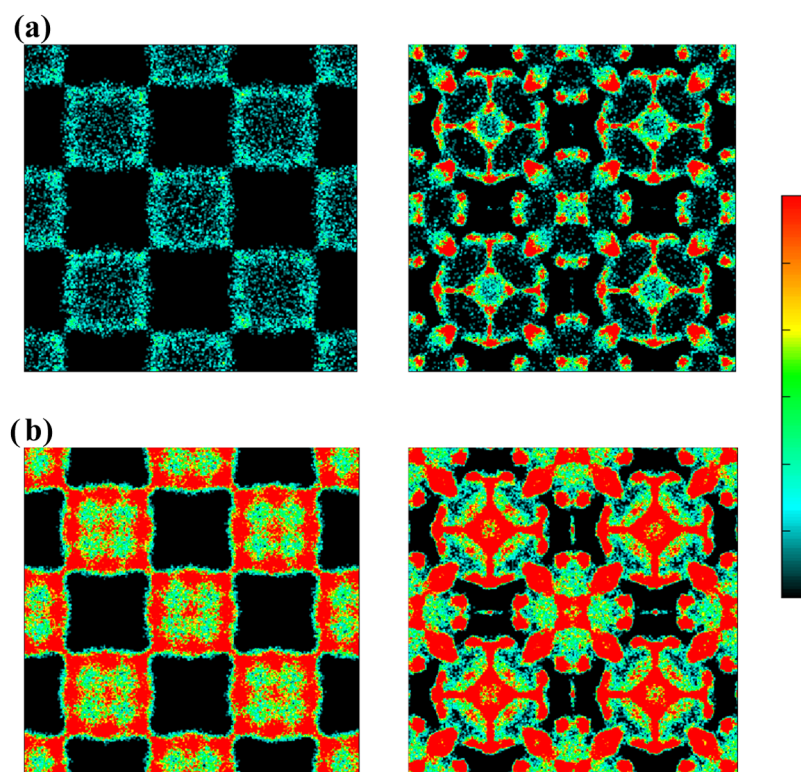
Figure 3. Calculated adsorption isotherms of (a) carbon dioxide, (b) methane, (c) carbon monoxide, (d) nitrogen, (e) oxygen, and (f) hydrogen on large-pore ZIF-7 (blue), ZIF-8 (orange), and ZIF-11 (gray) at 308 K up to 10 bar.

ZIF-7 has the same type of topology as ZIF-8 and possesses the same metal ion and ligand as ZIF-11. Using the new set of force field parameters, we obtained ZIF-7 adsorption isotherms that, at first sight, have significant discrepancies compared to experimental results. These discrepancies are attributed to the flexibility of the framework. ZIF-7 features structural flexibility and exhibits a narrow-to-large pore phase transition. This phase change can present gate opening or breathing effects that allow the adsorption of guest molecules that are larger than the diameter of its pore aperture.[29,74] Experimental isotherms exhibit a two-step sorption behavior for carbon dioxide and methane. At low pressures, the amount adsorbed increases linearly with pressure due to the limited surface area of the narrow-pore structure. A sharp uptake region is observed at high pressures due to the phase transition of the ZIF-7

structure from a narrow- to a large-pore state, indicating that CO_2 and CH_4 molecules were admitted to the internal cavities of the framework. The onset pressure of the structural transition for carbon dioxide is two orders of magnitude lower than the onset of methane due to the differences in molecule size and adsorption temperature. Using the new set of force field parameters, we simulated gas adsorption in both phases to account for the flexibility of the framework. The new force field agrees well with the lower part of isotherms but overpredicts carbon dioxide and methane adsorptions at the high-pressure range. The discrepancy at the upper part is attributed to the purity of the material. Insufficient solvent exchange time can lead to a reduction in pore volume and accessible surface area.[75]

Figure 4. Isosteric heats of adsorption at 1 bar (a) and 10 bar (b). Large-pore ZIF-7 (blue), ZIF-8 (orange), and ZIF-11 (gray).
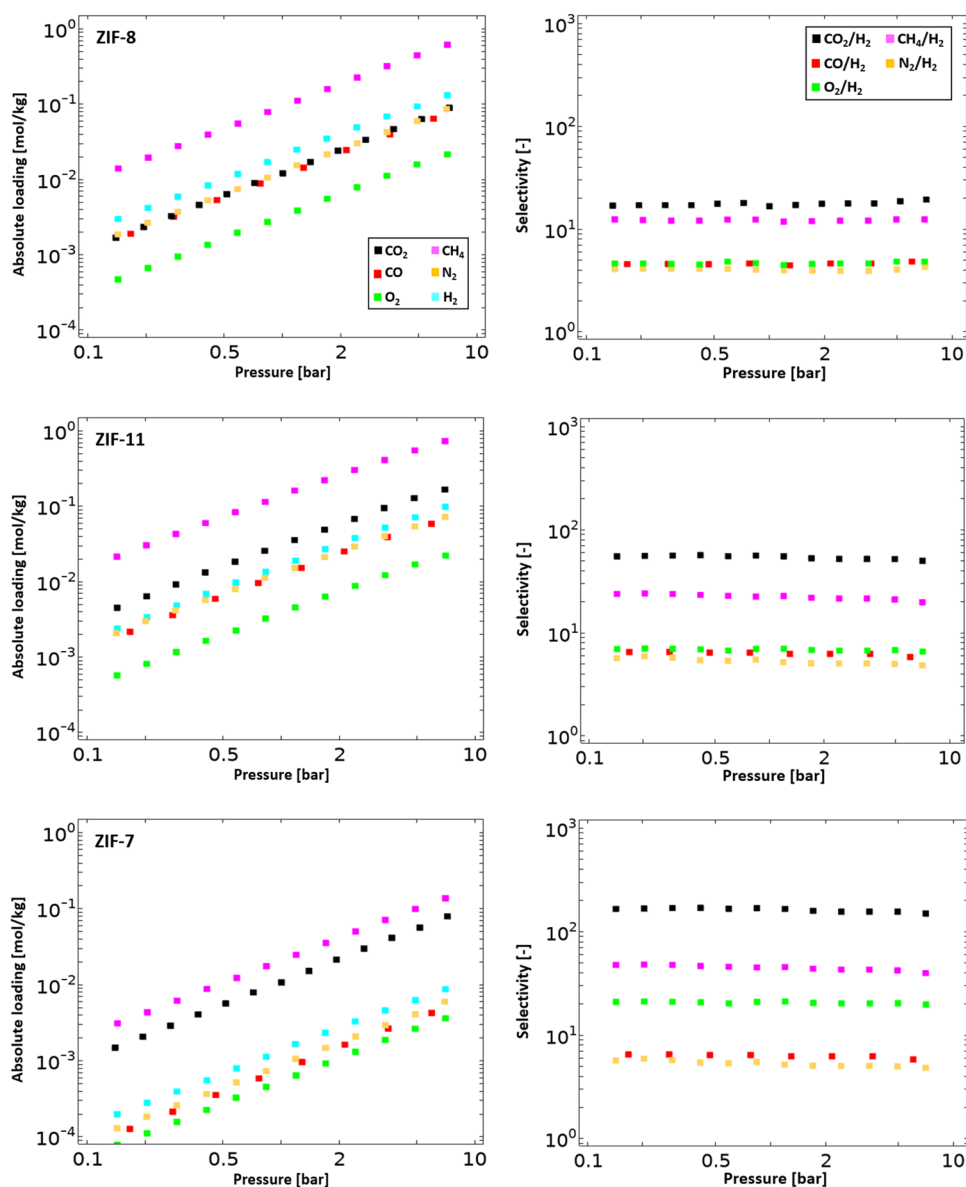

Figure 5. Average density profiles in ZIF-8 and ZIF-11 (from left to right) for carbon dioxide as a pure component at 1 bar (a) and 10 bar (b), and 308 K. The same color gradient (from dark to red) is employed in all figures. The dark area indicates a nonabsorbed site. The red area represents the most preferentially adsorbed site.

Both simulation and experiment exhibit a linear behavior for the adsorption of nitrogen in ZIF-7. This suggests that N_2 molecules do not induce the gate-opening effect upon the framework. Much lower measured nitrogen uptake is due to the external adsorption on ZIF-7 surfaces. The diameter of the pore aperture for ZIF-7 is smaller than the kinetic diameter of nitrogen, which means that the transport of N_2 molecules to the internal cavities is not possible without structural flexibility.[29,62,74] Klein et al.[73] reported isothermal measurements for hydrogen in ZIF-7 between 77 and 303 K. They found that a flexible model for hydrogen absorption is not needed for temperatures above 150 K, but pressure-induced phase change occurs upon the structure at a temperature below 123 K. The simulation results for hydrogen and nitrogen follow the trend of the experimental results but slightly underestimate

the values. The difference is most likely ascribed to the fact that the experiment measured a narrow-pore structure having a slightly higher surface area than the narrow-pore phase used in this work. To the best of our knowledge, there are no measured isotherms for carbon monoxide and oxygen in ZIF-7 and ZIF-11. Therefore, adsorption behaviors for these two gases are calculated using our GCMC simulation and compared with other gases in the pure-component results of the next section.

Pure-Component Adsorption. Using the validated set of force-field parameters, adsorption isotherms of carbon dioxide, methane, carbon monoxide, nitrogen, oxygen, and hydrogen in ZIF-7, ZIF-8, and ZIF-11 are computed at 308 K (Figure 3). The simulations indicate that carbon dioxide is preferentially adsorbed in all of the ZIFs, followed by the adsorption of
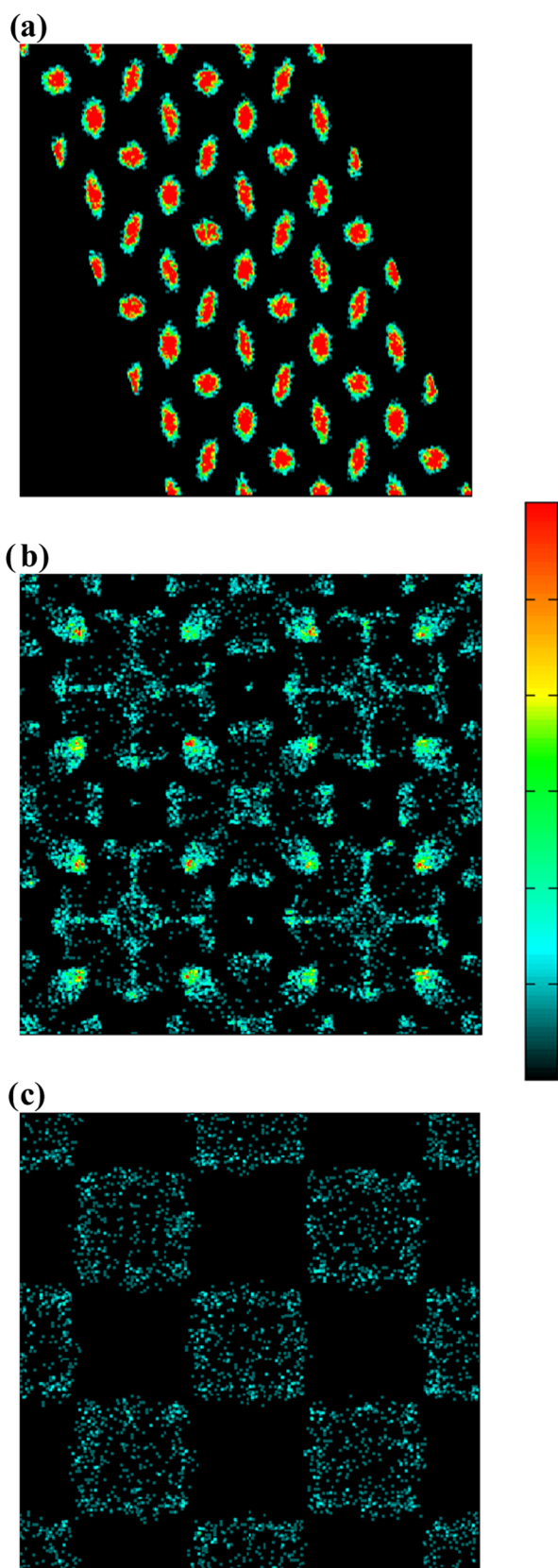
Figure 6. Calculated six-component adsorption isotherms (left) and selectivity (right) in ZIF-8, ZIF-11, and narrow-pore ZIF-7 at 308 K: 58 mol % H_2 (cyan), 22 mol % CH_4 (magenta), 9 mol % N_2 (orange), 7 mol % CO (red), 2 mol % CO_2 (black), and 2 mol % O_2 (green).

methane. The results for nitrogen, carbon monoxide, and oxygen show almost the same adsorption behavior. Hydrogen is the least adsorbed component. Many studies reported that gas adsorption strength on MOFs follows the order (CO_2 > CH_4 > CO > N_2 > H_2).[33,72,79,83,84] The difference in the adsorption strength of these gases can be explained by their polarizability and dipole/quadrupole moments.[85] It is clear that the loading of these molecules in ZIFs follows the order of their polarizability rather than dipole or quadrupole (Table 2). At low pressures (<0.5 bar), uptakes of carbon dioxide and methane in ZIF-7 are significantly higher than those in ZIF-11 and ZIF-8, ascribed to the fact that our rigid force-field parameters are not able to predict the framework flexibility of ZIF-7 topology in the narrow-pore phase. It is worth noting that isotherms for carbon monoxide and oxygen in ZIF-7 show the same behavior as its rigid counterpart (i.e., ZIF-11), implying that the rigid force field can predict CO and O_2 adsorptions in ZIF-7 either in low or high-pressure range. The uptake for carbon dioxide in ZIF-8 and ZIF-11 increases

sharply and surpasses the adsorption of ZIF-7 at the crossover pressure of 4 bar, after which ZIF-8 reaches the highest adsorption at 10 bar. The crossover implies that CO_2 adsorption is strongly affected by ZIF topology.

To understand this topological effect, isosteric heats of adsorption on ZIFs are calculated at different pressures in Figure 4. As expected, isosteric heats of adsorbed gases follow the order of gas polarizability. ZIF-7 exhibits a much higher heat of adsorption than ZIF-8 and ZIF-11. Morris et al.[38] reported CO_2 adsorption experiments where topologies (ZIF-7 and 94) with smaller pores have larger adsorptions than their counterparts (ZIF-11 and 93, respectively) at a pressure below 1 bar. The reverse occurs at higher pressures (>10 bar), where the larger-pore structures (ZIF-11 and 93) have significantly higher adsorption. Their experiments are in agreement with our simulation results. This suggests that narrow-size topology provides a stronger binding environment to interact with adsorbates, but gas adsorption can be limited at high pressure due to a low accessible surface area. It appears that carbon
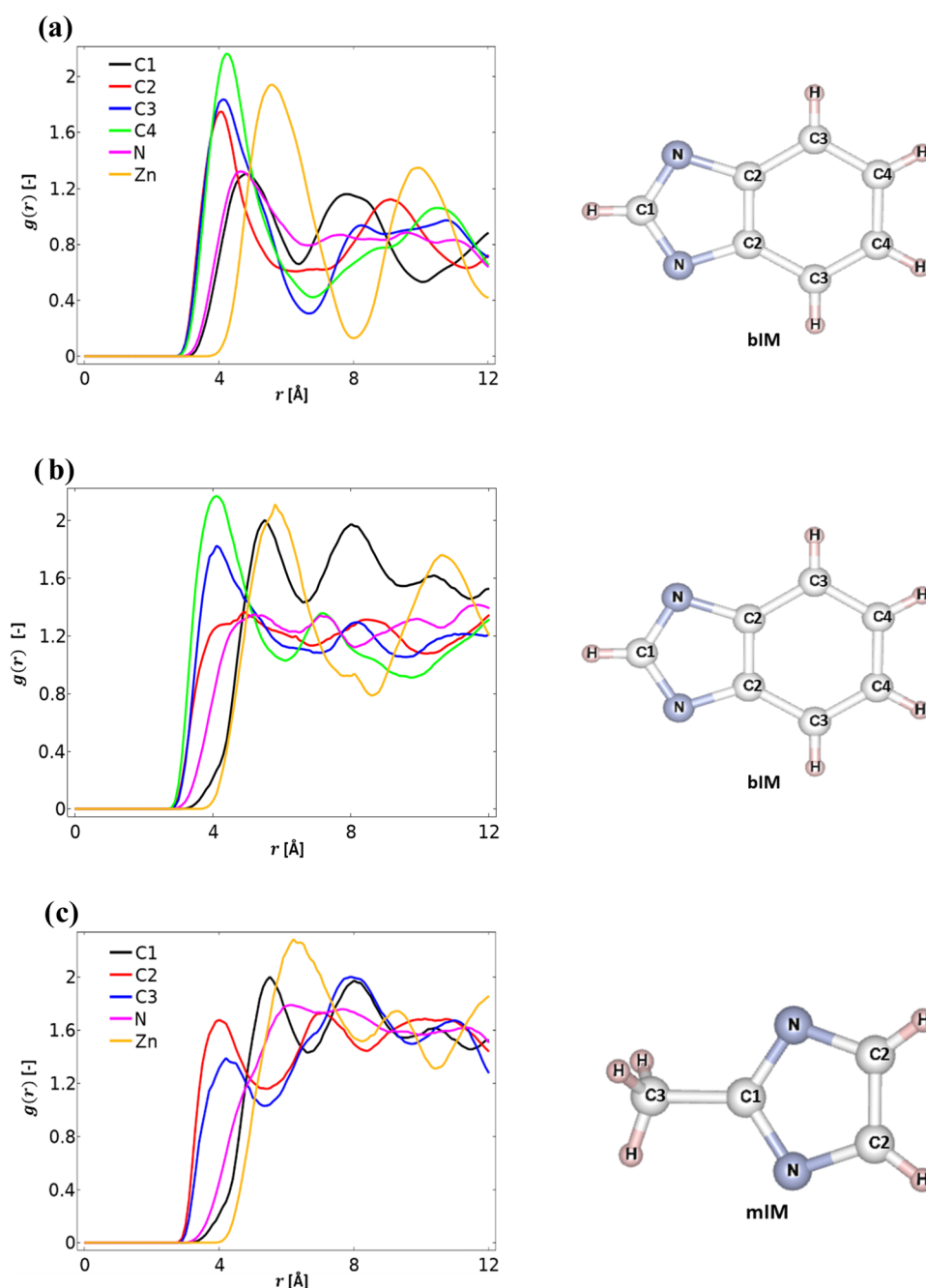
(a)

(b)

(c)

Figure 7. Average density profiles of carbon monoxide adsorption from the quaternary mixture in large-pore ZIF-7 (a), ZIF-11 (b), and ZIF-8 (c) at the total gas pressure of 10 bar and 308 K.

monoxide, nitrogen, and oxygen are not sensitive to the surface area but strongly depend on the pore size since they are preferentially adsorbed in a narrow-pore topology (ZIF-7). It is worth noticing that ZIF-7 (bIM) and ZIF-8 (mIM) have different Imidazolate linkers. The effect of ligands can also play a role in the adsorption behaviors. Since ZIF-11 (bIM) and ZIF-8 (mIM) have similar pore sizes and surface areas, the difference in the heat of adsorption between ZIF-11 (bIM) and ZIF-8 (mIM) can be mainly attributed to the interaction of gas molecules with different ligands. COG generally interacts stronger with bIM ligand at 1 bar, but this does not guarantee a high CO_2 uptake at a higher pressure (10 bar). It can also be seen that adsorption isotherms of ZIF-11 (bIM) and ZIF-8 (mIM) show almost the same uptakes for methane, carbon monoxide, nitrogen, oxygen, and hydrogen. It is, therefore, safe to assume that the effect of Imidazolate linkers can be ignored on the adsorption behaviors of COG in ZIF-7 (bIM), ZIF-8 (mIM), and ZIF-11 (bIM).

The crossover behavior for the adsorption of carbon dioxide is also observed in large-pore structures (ZIF-8 *vs* ZIF-11), although their topologies have similar surface areas. We found that the reverse of gas adsorption from ZIF-11 to ZIF-8 is difficult to be related to the effect of the organic linker and pore size. Therefore, average occupation profiles (Figure 5) are obtained to understand this reverse behavior for CO_2 adsorption in ZIF-8 and ZIF-11. These profiles are calculated from the average values (averaged over the whole number of configurations of the simulations) of the projections of the center of mass coordinates over the $x-y$ plane, indicating sites where guest molecules are preferentially adsorbed. In ZIF-8, guest molecules at low pressure are mainly located in the pore volume. In ZIF-11, a significant amount of the adsorption takes place at sites close to narrow-size channels in the *lta*-cages and six-membered ring windows between the cages. The reverse occurs at higher pressure, where the adsorption sites for carbon dioxide in ZIF-11 quickly reach their capacity in the pore channels and organic ring windows. While large surface area and pore volume contribute to the high retention of gas molecules in SOD topology, leading to a strong interaction between the adsorbate and the framework at high pressure. Methane, carbon monoxide, and hydrogen follow similar behaviors, adsorbing preferentially in organic rings and narrow-size channels (shown in Figure S4). Houndonougbo et al.[61] studied methane adsorption in a series of ZIFs built by RHO topology and found that the binding site is confined to the six-membered, eight-membered, and four-membered rings. Han et al.[40] studied six ZIF topologies (*i.e.*, BCT, DFT, SOD, MER, RHO, GME). Their work suggests that the adsorption behavior is determined by the surface area and pore size rather than the topology, but adsorption sites depend strongly on topology. In fact, Zeolitic topologies are quite extensive (105 ZIFs with 38 topological codes).[86] Some ZIFs have the same topology but very different pore shapes and sizes. Many topologies do not seem to share prominent features to explain their adsorption performances. Martin-Calvo et al.[56] screened 218 zeolites and studied the effect of material topology on hydrogen adsorption capacity. They pointed out that some of the topologies have certain similarities, but, in general, they are quite different. We believe that the effect of ZIF topology on the adsorption behaviors of these gases is mainly attributed to their topologies having different pore sizes, surface areas, and adsorption sites.
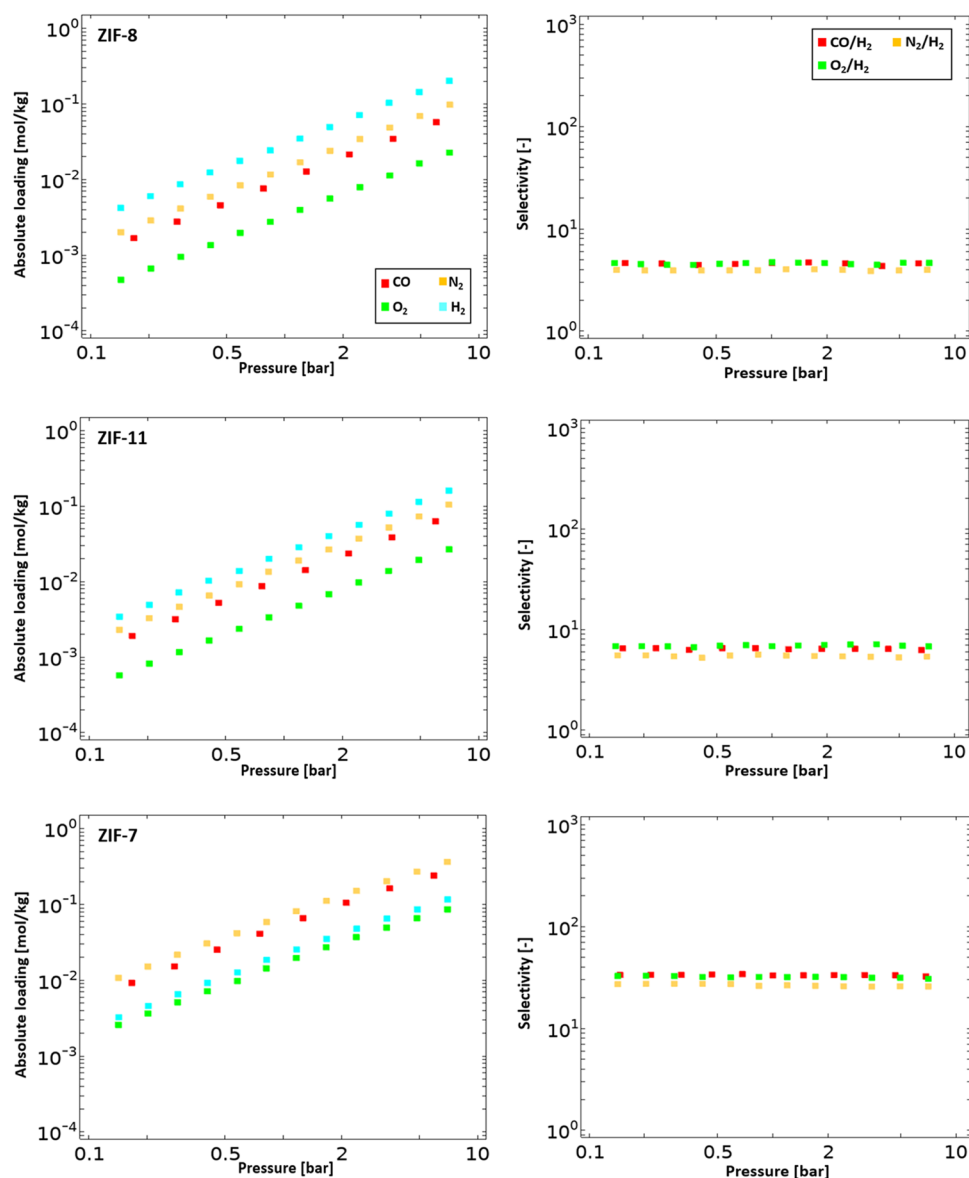
Multicomponent Adsorption. Many studies indicate that ZIFs can efficiently separate carbon dioxide from ternary mixtures[20,87] ($CO_2/N_2/H_2O$ and $CO_2/CH_4/H_2O$) or binary

Figure 8. Radial distribution functions for carbon monoxide around the framework atoms of ZIF-7 (a), ZIF-11 (b), and ZIF-8 (c). The interaction of carbon monoxide to carbon atoms (C1 in black, C2 in red, C3 in blue, and C4 in green) of bIM linker in ZIF-7 and ZIF-11. The interaction between CO and carbon atoms (C1 in black, C2 in red, C3 in blue) of mIM linker in ZIF-8. The interactions with nitrogen atoms (magenta) and zinc metal (orange).

mixtures[29,30,38,88] such as CO_2/H_2, CO_2/N_2, CO_2/CO, and CO_2/CH_4 due to carbon dioxide having higher polarizability than other gases. The removal of other contaminants is also of great importance. Unfortunately, almost all of the reported experiments and simulations focus on pure-component gas and binary mixture. The fact is that multicomponent gas mixture studies for separation are much scarcer due to the complexity of the systems. In this regard, we performed a series of GCMC simulations to investigate the adsorption and separation of COG with a simplified composition containing hydrogen (58 mol %), methane (22 mol %), nitrogen (9 mol %), carbon monoxide (7 mol %), and carbon dioxide (2 mol %), and oxygen

(2 mol %). This work considers the adsorption and separation of COG in a rigid framework. According to force-field validation, ZIF-11 and ZIF-8 do not exhibit a phase-transition framework flexibility. In contrast, ZIF-7 undergoes a significant structural transition from low to high pressure upon adsorption of CH_4 and CO_2. To study the impact of topology on the separation performance, we compare ZIF-7 at a narrow-pore phase to ZIF-11 and ZIF-8 since the gas partial pressures of carbon dioxide and methane are lower than the onset pressure of the structural transition Figure 6 illustrates the adsorption isotherms of the COG mixture and the corresponding selectivity of each component to hydrogen. Methane shows

Figure 9. Simulated quaternary mixture adsorption isotherms (left) and selectivity (right) in ZIF-8, ZIF-11, and ZIF-7 at 308 K: 82 mol % H_2, 10 mol % N_2, 6 mol % CO, and 2 mol % O_2.

significantly higher adsorption than other components, attributed to a large molar fraction in the presence of the mixture. Although much less carbon dioxide is adsorbed than methane, the highest selectivity is observed on CO_2/H_2. The size of the pores in a material determines its selectivity for hydrogen separation and adsorption capacity. Materials with smaller pore sizes exhibit higher selectivity but lower adsorption, while larger pore sizes provide higher adsorption but lower selectivity. In the case of ZIF-7, with a pore size of approximately 4 Å, it exhibits high selectivity for H_2 separation from COG, but the adsorption is an order of magnitude lower than the other two. On the other hand, ZIF-8, with a pore size of about 11 Å, shows higher adsorption capacity but much lower selectivity for hydrogen separation. ZIF-11 has a broader PSD than ZIF-7, with pore sizes ranging from 6.22 Å (*d8r-*cage) to 14.17 Å (*lta-*cage), which may seem advantageous. The separation performance lies between ZIF-7 and ZIF-8, but it can adsorb COG as much as ZIF-8 due to its larger surface area. Pure-component simulation previously showed that ZIF-

8 has higher CO_2 and CH_4 adsorption than ZIF-11 at 10 bar, but ZIF-11 performs better than ZIF-8 in terms of gas separation. This is because partial gas pressures for CO_2 and CH_4 are much lower than the crossover pressure (a total gas pressure of 10 bar for the mixture). ZIF-11 topology favors stronger adsorbate binding below the crossover pressure, thus leading to better performance than ZIF-8. It is also interesting to note that the selectivity for CO_2/H_2 and CH_4/H_2 for ZIF-11 and ZIF-7 drops slightly with the increase of the total gas pressure, possibly ascribed to the packing effect.[36,43] At high pressure, the packing effect tends to favor the adsorption of smaller molecules in narrow-size adsorption sites. This can result in reduced selectivity for larger molecules like CH_4 and CO_2 over hydrogen. However, ZIF-8 is not susceptible to this effect since gas adsorption primarily occurs in the pore cage at low pressure, minimizing the impact of hydrogen packing.

Carbon monoxide is the most problematic contaminant for catalysts in fuel cells. However, ZIF-11 and ZIF-8 do not show any advantage in separating hydrogen from low-polarizability

molecules (*e.g.*, CO, N_2, and O_2) in the COG mixture. In this regard, a new composition is considered by assuming that the most adsorbed species (*i.e.*, CO_2 and CH_4) are completely removed, thus resulting in a quaternary mixture having hydrogen (86 mol %), carbon monoxide (6 mol %), nitrogen (10 mol %), and oxygen (2 mol %). Since this mixture does not induce ZIFs flexibility, we can compare the separation performances of large-pore ZIF-7, ZIF-8, and ZIF-11. The average density profiles (Figure 7) show that carbon monoxide is favorably adsorbed in narrow pore cages of ZIF-7 compared to ZIF-8 and ZIF-11 representing large-pore topologies. The density distributions of nitrogen and oxygen follow a similar trend to the adsorption of carbon monoxide in ZIFs. As discussed, a narrow-size pore can provide a stronger binding environment to interact with the adsorbates. Wu et al.[36] concluded that stronger adsorption affinity is attributed to the enhanced interaction between adsorbates and the specific group of organic linkers in smaller pore sizes. For a deeper understanding of the enhanced binding of carbon monoxide in the narrow-size pore, we analyze the radial distribution functions (RDFs) of the CO molecule to each atom of three ZIFs (Figure 8). Pronounced peaks in the RDFs of ZIF-7 are observed for CO around C2 (4.09 Å), C3 (4.14 Å), and C4 (4.26 Å) atoms, followed by C1 (4.81 Å) and N atoms (4.64 Å). The furthest peak is at 5.53 Å for Zn. This implies that CO molecules are proximal to the ring formed by the C═C bond of organic linkers. As opposed to ZIF-7, the peaks of CO around C2 and N atoms disappear in the RDFs of ZIF-11. This suggests that the narrow-size pore of ZIF-7 enhances the interactions of CO around C2═N and C2═C2 bonds. Despite a different imidazolate linker (mIM) in ZIF-8, its large-pore topology does not favor the binding on C1═N (4.08 Å for C2, 4.21 Å for C3, 5.51 Å for C1, and 6.05 Å for N). The separation performances of ZIF-7, ZIF-8, and ZIF-11 are also compared in terms of adsorption selectivity (Figure 9). ZIF-7 exhibits the best performance in separating hydrogen from carbon monoxide (up to 30) due to the enhanced binding in narrow-size topology. The selectivity of CO/H_2 reaches slightly higher than N_2/H_2 and O_2/H_2. The difference may be because carbon monoxide has a dipole moment resulting in slightly stronger interaction in a narrow-pore structure than nonpolar molecules like nitrogen and oxygen. However, the weak affinity of frameworks to carbon monoxide leads to the difficulty of complete gas retention from multicomponent mixtures. It would be more interesting to use ZIF-7 and ZIF-11 as sieving membranes since their pore apertures are similar to the kinetic diameter of H_2 (2.89 Å) but smaller than the size of the CO molecule (3.76 Å). The diffusion rates of gas molecules are also determined by topological properties (*e.g.*, pore shape, size, surface area) and structural flexibility. The effect of ZIF topology and flexibility on hydrogen separation from COG in ZIF-based sieve membranes will be future work for the next step.

CONCLUSIONS

This molecular simulations study aims to assess the effectiveness of ZIF-7, ZIF-8, and ZIF-11 in purifying hydrogen from COG. Our findings revealed that the separation performance of hydrogen from carbon dioxide is heavily dependent on topology due to its high polarizability, as evidenced by the reverse behavior observed in adsorption isotherms and heats of adsorption. The difference in separation performance between ZIF-11 and ZIF-8 (large pore structures)

can be attributed to their topologies and the presence of different adsorption sites. The average density profiles demonstrated that COG prefers to adsorb in narrow-size pore channels formed by imidazolate rings in RHO topology, whereas gas adsorption mainly occurs in the cages of SOD topology, resulting in weaker interaction at low pressure. For the quaternary mixture of gases, we found that a narrow-pore topology facilitated a stronger binding, leading to an improved separation performance. The radial distribution functions further revealed that the interactions of CO around C2═N and C2═C2 bonds were enhanced in the hexagonal sod-cage of ZIF-7, while cubic SOD and RHO topologies were less conducive to CO binding on the C═N bond. Our results suggest that a large-pore topology having narrow-size adsorption sites and high surface area is beneficial for separating hydrogen from CO_2 and methane. On the other hand, to separate hydrogen from CO, O_2, and N_2, a narrow-pore topology facilitates a stronger binding with impurities to enhance purification performance.

■ ASSOCIATED CONTENT

Ⓢ Supporting Information

The Supporting Information is available free of charge at https://pubs.acs.org/doi/10.1021/acssuschemeng.2c07006.

> Atomic charges of metal center, mIM and bIM linkers, and rescaling UFF parameters to reproduce the adsorption isotherms of CO_2 in ZIF-8 at 273 K (S1); comparison between the experimental (open) and calculated (closed) adsorption isotherms of CO in ZIF-8 (S2); average density profiles of hydrogen, carbon monoxide, and methane in large-pore ZIF-7, Z-8, and ZIF-11 (S3) (PDF)

■ AUTHOR INFORMATION

Corresponding Authors

Ana Martín-Calvo — *Department of Physical, Chemical and Natural Systems, University Pablo de Olavide, 41013 Seville, Spain;* ⊙ orcid.org/0000-0002-0284-6777; Email: amarcal@upo.es

Sofía Calero — *Department of Applied Physics, Eindhoven University of Technology, Eindhoven 5600 MB, The Netherlands;* ⊙ orcid.org/0000-0001-9535-057X; Email: s.calero@tue.nl

Authors

Xiucheng Huang — *Department of Applied Physics, Eindhoven University of Technology, Eindhoven 5600 MB, The Netherlands*

Martijn J. J. Mulder — *HyET Hydrogen B.V., Arnhem 6827 AV, The Netherlands*

Sjoerd C. J. van Acht — *HyET Hydrogen B.V., Arnhem 6827 AV, The Netherlands*

Juan José Gutiérrez-Sevillano — *Department of Physical, Chemical and Natural Systems, University Pablo de Olavide, 41013 Seville, Spain;* ⊙ orcid.org/0000-0001-8224-839X

Julio C. García-Navarro — *Stichting New Energy Coalition, 9747 AG Groningen, The Netherlands*

Complete contact information is available at:
https://pubs.acs.org/10.1021/acssuschemeng.2c07006

Notes

The authors declare no competing financial interest.

■ REFERENCES

(1) Relvas, F.; Whitley, R. D.; Silva, C.; Mendes, A. Single-Stage Pressure Swing Adsorption for Producing Fuel Cell Grade Hydrogen. *Ind. Eng. Chem. Res.* **2018**, *57*, 5106−5118.

(2) Gao, F.; Wang, S.; Wang, W.; Duan, J.; Dong, J.; Chen, G. Adsorption separation of CO from syngas with CuCl@AC adsorbent by a VPSA process. *RSC Adv.* **2018**, *8*, 39362−39370.

(3) Bacquart, T.; Arrhenius, K.; Persijn, S.; Rojo, A.; Auprêtre, F.; Gozlan, B.; Moore, N.; Morris, A.; Fischer, A.; Murugan, A.; Bartlett, S.; Doucet, G.; Laridant, F.; Gernot, E.; Fernández, T. E.; Gómez, C.; Carré, M.; De Reals, G.; Haloua, F. Hydrogen fuel quality from two main production processes: Steam methane reforming and proton exchange membrane water electrolysis. *J. Power Sources* **2019**, *444*, No. 227170.

(4) Nikolaidis, P.; Poullikkas, A. A comparative overview of hydrogen production processes. *Renewable Sustainable Energy Rev.* **2017**, *67*, 597−611.

(5) Van Acht, S.C.J.; Laycock, C.; Carr, S.J.W.; Maddy, J.; Guwy, A. J.; Lloyd, G.; Raymakers, L.F.J.M. Simulation of integrated novel PSA/EHP/C process for high-pressure hydrogen recovery from Coke Oven Gas. *Int. J. Hydrogen Energy* **2020**, *45*, 15196−15212.

(6) Van Acht, S.C.J.; Laycock, C. J.; Carr, S.J.W.; Maddy, J.; Guwy, A. J.; Lloyd, G.; Raymakers, L.F.J.M.; Wright, A. D. Optimization of VPSA-EHP/C process for high-pressure hydrogen recovery from Coke Oven Gas using CO selective adsorbent. *Int. J. Hydrogen Energy* **2021**, *46*, 709−725.

(7) Razzaq, R.; Li, C.; Zhang, S. Coke oven gas: Availability, properties, purification, and utilization in China. *Fuel* **2013**, *113*, 287−299.

(8) Bermúdez, J. M.; Arenillas, A.; Luque, R.; Menéndez, J. A. An overview of novel technologies to valorise coke oven gas surplus. *Fuel Process. Technol.* **2013**, *110*, 150−159.

(9) Papadias, D. D.; Ahmed, S.; Kumar, R.; Joseck, F. Hydrogen quality for fuel cell vehicles − A modeling study of the sensitivity of impurity content in hydrogen to the process variables in the SMR−PSA pathway. *Int. J. Hydrogen Energy* **2009**, *34*, 6021−6035.

(10) Nordio, M.; Eguaras Barain, M.; Raymakers, L.; Van Sint Annaland, M.; Mulder, M.; Gallucci, F. Effect of CO_2 on the performance of an electrochemical hydrogen compressor. *Chem. Eng. J.* **2020**, *392*, No. 123647.

(11) Brunetti, A.; Barbieri, G.; Drioli, E. A PEMFC and H_2 membrane purification integrated plant. *Chem. Eng. Process.* **2008**, *47*, 1081−1089.

(12) Silva, B.; Solomon, I.; Ribeiro, A. M.; Lee, U.-H.; Hwang, Y. K.; Chang, J.-S.; Loureiro, J. M.; Rodrigues, A. E. H_2 purification by pressure swing adsorption using CuBTC. *Sep. Purif. Technol.* **2013**, *118*, 744−756.

(13) Xiao, J.; Peng, Y.; Bénard, P.; Chahine, R. Thermal effects on breakthrough curves of pressure swing adsorption for hydrogen purification. *Int. J. Hydrogen Energy* **2016**, *41*, 8236−8245.

(14) Lee, J.; Kim, M.; Lee, D.; Ahn, H.; Kim, M.; Lee, C. Heat-exchange pressure swing adsorption process for hydrogen separation. *AIChE J.* **2008**, *54*, 2054−2064.

(15) Xiao, J.; Li, R.; Bénard, P.; Chahine, R. Heat and mass transfer model of multicomponent adsorption system for hydrogen purification. *Int. J. Hydrogen Energy* **2015**, *40*, 4794−4803.

(16) Férey, G.; Serre, C.; Devic, T.; Maurin, G.; Jobic, H.; Llewellyn, P. L.; De Weireld, G.; Vimont, A.; Daturi, M.; Chang, J.-S. Why hybrid porous solids capture greenhouse gases. *Chem. Soc. Rev.* **2011**, *40*, 550−562.

(17) Lopes, F. V.; Grande, C. A.; Rodrigues, A. E. Activated carbon for hydrogen purification by pressure swing adsorption: Multi-component breakthrough curves and PSA performance. *Chem. Eng. Sci.* **2011**, *66*, 303−317.

(18) Reed, D. A.; Xiao, D. J.; Gonzalez, M. I.; Darago, L. E.; Herm, Z. R.; Grandjean, F.; Long, J. R. Reversible CO Scavenging via Adsorbate-Dependent Spin State Transitions in an Iron(II)−Triazolate Metal−Organic Framework. *J. Am. Chem. Soc.* **2016**, *138*, 5594−5602.

(19) Evans, A.; Luebke, R.; Petit, C. The use of metal−organic frameworks for CO purification. *J. Mater. Chem. A* **2018**, *6*, 10570−10594.

(20) Liu, B.; Smit, B. Molecular Simulation Studies of Separation of CO_2/N_2, CO_2/CH_4, and CH_4/N_2 by ZIFs. *J. Phys. Chem. C* **2010**, *114*, 8515−8522.

(21) Avci, G.; Erucar, I.; Keskin, S. Do New MOFs Perform Better for CO_2 Capture and H_2 Purification? Computational Screening of the Updated MOF Database. *ACS Appl. Mater. Interfaces* **2020**, *12*, 41567−41579.

(22) Liu, H.; Cheng, M.; Liu, Y.; Wang, J.; Zhang, G.; Li, L.; Du, L.; Wang, G.; Yang, S.; Wang, X. Single atoms meet metal−organic frameworks: collaborative efforts for efficient photocatalysis. *Energy Environ. Sci.* **2022**, *15*, 3722−3749.

(23) Thornton, A. W.; Dubbeldam, D.; Liu, M. S.; Ladewig, B. P.; Hill, A. J.; Hill, M. R. Feasibility of zeolitic imidazolate framework membranes for clean energy applications. *Energy Environ. Sci.* **2012**, *5*, 7637.

(24) Nishiyama, N.; Yamaguchi, M.; Katayama, T.; Hirota, Y.; Miyamoto, M.; Egashira, Y.; Ueyama, K.; Nakanishi, K.; Ohta, T.; Mizusawa, A.; Satoh, T. Hydrogen-permeable membranes composed of zeolite nano-blocks. *J. Membr. Sci.* **2007**, *306*, 349−354.

(25) Ma, X.; Wu, X.; Caro, J.; Huang, A. Polymer Composite Membrane with Penetrating ZIF-7 Sheets Displays High Hydrogen Permselectivity. *Angew. Chem., Int. Ed.* **2019**, *58*, 16156−16160.

(26) Yang, T.; Shi, G. M.; Chung, T.-S. Symmetric and Asymmetric Zeolitic Imidazolate Frameworks (ZIFs)/Polybenzimidazole (PBI) Nanocomposite Membranes for Hydrogen Purification at High Temperatures. *Adv. Energy Mater.* **2012**, *2*, 1358−1367.

(27) Song, Q.; Nataraj, S. K.; Roussenova, M. V.; Tan, J. C.; Hughes, D. J.; Li, W.; Bourgoin, P.; Alam, M. A.; Cheetham, A. K.; Al-Muhtaseb, S. A.; Sivaniah, E. Zeolitic imidazolate framework (ZIF-8) based polymer nanocomposite membranes for gas separation. *Energy Environ. Sci.* **2012**, *5*, 8359.

(28) Kumar, R.; Kumar, M.; Awasthi, K. Nanoporous Polymeric Membranes for Hydrogen Separation. In *Nanotechnology for Energy and Environmental Engineering*; Springer, 2021; pp 355−376.

(29) Arami-Niya, A.; Birkett, G.; Zhu, Z.; Rufford, T. E. Gate opening effect of zeolitic imidazolate framework ZIF-7 for adsorption of CH_4 and CO_2 from N_2. *J. Mater. Chem. A* **2017**, *5*, 21389−21399.

(30) Cacho-Bailo, F.; Matito-Martos, I.; Perez-Carbajo, J.; Etxeberría-Benavides, M.; Karvan, O.; Sebastián, V.; Calero, S.; Téllez, C.; Coronas, J. On the molecular mechanisms for the H_2/CO_2 separation performance of zeolite imidazolate framework two-layered membranes. *Chem. Sci.* **2017**, *8*, 325−333.

(31) Namsani, S.; Ozcan, A.; Yazaydın, A.Ö. Direct Simulation of Ternary Mixture Separation in a ZIF-8 Membrane at Molecular Scale. *Adv. Theory Simul.* **2019**, *2*, No. 1900120.

(32) Ania, C. O.; García-Pérez, E.; Haro, M.; Gutiérrez-Sevillano, J. J.; Valdés-Solís, T.; Parra, J. B.; Calero, S. Understanding Gas-Induced Structural Deformation of ZIF-8. *J. Phys. Chem. Lett.* **2012**, *3*, 1159−1164.

(33) Wang, B.; Côté, A. P.; Furukawa, H.; O'Keeffe, M.; Yaghi, O. M. Colossal cages in zeolitic imidazolate frameworks as selective carbon dioxide reservoirs. *Nature* **2008**, *453*, 207−211.

(34) Banerjee, R.; Phan, A.; Wang, B.; Knobler, C.; Furukawa, H.; O'Keeffe, M.; Yaghi, O. M. High-Throughput Synthesis of Zeolitic Imidazolate Frameworks and Application to CO_2 Capture. *Science.* **2008**, *319*, 939−943.

(35) Park, K. S.; Ni, Z.; Cote, A. P.; Choi, J. Y.; Huang, R.; Uribe-Romo, F. J.; Chae, H. K.; O'Keeffe, M.; Yaghi, O. M. Exceptional

chemical and thermal stability of zeolitic imidazolate frameworks. *Proc. Natl. Acad. Sci. U.S.A.* **2006**, *103*, 10186−10191.

(36) Wu, Y.; Chen, H.; Liu, D.; Qian, Y.; Xi, H. Adsorption and separation of ethane/ethylene on ZIFs with various topologies: Combining GCMC simulation with the ideal adsorbed solution theory (IAST). *Chem. Eng. Sci.* **2015**, *124*, 144−153.

(37) Yun, J.-H.; He, Y.; Otero, M.; Düren, T.; Seaton, N. A. In Adsorption Equilibrium of Polar/non-polar Mixtures on MCM-41: Experiments And Monte Carlo Simulation. *Characterization of Porous Solids VI, Proceedings of the 6th International Symposium on the Characterization of Porous Solids (COPS-VI)*, Elsevier, 2002; pp 685−692.

(38) Morris, W.; He, N.; Ray, K. G.; Klonowski, P.; Furukawa, H.; Daniels, I. N.; Houndonougbo, Y. A.; Asta, M.; Yaghi, O. M.; Laird, B. B. A Combined Experimental-Computational Study on the Effect of Topology on Carbon Dioxide Adsorption in Zeolitic Imidazolate Frameworks. *J. Phys. Chem. C* **2012**, *116*, 24084−24090.

(39) Gao, M.; Wang, J.; Rong, Z.; Shi, Q.; Dong, J. A combined experimental-computational investigation on water adsorption in various ZIFs with the SOD and RHO topologies. *RSC Adv.* **2018**, *8*, 39627−39634.

(40) Han, S. S.; Choi, S.-H.; Goddard, W. A. Zeolitic Imidazolate Frameworks as H_2 Adsorbents: Ab Initio Based Grand Canonical Monte Carlo Simulation. *J. Phys. Chem. C* **2010**, *114*, 12039−12047.

(41) Dubbeldam, D.; Calero, S.; Ellis, D. E.; Snurr, R. Q. RASPA: molecular simulation software for adsorption and diffusion in flexible nanoporous materials. *Mol. Simul.* **2016**, *42*, 81−101.

(42) Li, Q.; Ruan, M.; Lin, B.; Zhao, M.; Zheng, Y.; Wang, K. Molecular simulation study of metal organic frameworks for methane capture from low-concentration coal mine methane gas. *J. Porous Mater.* **2016**, *23*, 107−122.

(43) Guo, H.; Shi, F.; Ma, Z.; Liu, X. Molecular Simulation for Adsorption and Separation of CH_4/H_2 in Zeolitic Imidazolate Frameworks. *J. Phys. Chem. C* **2010**, *114*, 12158−12165.

(44) Peng, D.-Y.; Robinson, D. B. A New Two-Constant Equation of State. *Ind. Eng. Chem. Fund.* **1976**, *15*, 59−64.

(45) Dubbeldam, D.; Calero, S.; Vlugt, T.J.H.; Snurr, R. Q. Molecular Simulations of Adsorption and Diffusion in Crystalline Nanoporous Materials. *Handbook of Porous Materials*, 2021; pp 199−319.

(46) Zhou, W.; Wu, H.; Hartman, M. R.; Yildirim, T. Hydrogen and Methane Adsorption in Metal−Organic Frameworks: A High-Pressure Volumetric Study. *J. Phys. Chem. C* **2007**, *111*, 16131−16137.

(47) Gatica, S.; Nekhai, A.; Scrivener, A. Adsorption and Gas Separation of Molecules by Carbon Nanohorns. *Molecules* **2016**, *21*, 662.

(48) Harris, J. G.; Yung, K. H. Carbon Dioxide's Liquid-Vapor Coexistence Curve And Critical Properties as Predicted by a Simple Molecular Model. *J. Phys. Chem. A* **1995**, *99*, 12021−12024.

(49) García-Sánchez, A.; Ania, C. O.; Parra, J. B.; Dubbeldam, D.; Vlugt, T.J.H.; Krishna, R.; Calero, S. Transferable Force Field for Carbon Dioxide Adsorption in Zeolites. *J. Phys. Chem. C* **2009**, *113*, 8814−8820.

(50) Calero, S.; Dubbeldam, D.; Krishna, R.; Smit, B.; Vlugt, T.J.H.; Denayer, J.F.M.; Martens, J. A.; Maesen, T.L.M. Understanding the Role of Sodium during Adsorption: A Force Field for Alkanes in Sodium-Exchanged Faujasites. *J. Am. Chem. Soc.* **2004**, *126*, 11377−11386.

(51) Martin-Calvo, A.; Gutiérrez-Sevillano, J. J.; Parra, J. B.; Ania, C. O.; Calero, S. Transferable force fields for adsorption of small gases in zeolites. *Phys. Chem. Chem. Phys.* **2015**, *17*, 24048−24055.

(52) Deeg, K. S.; Gutiérrez-Sevillano, J. J.; Bueno-Pérez, R.; Parra, J. B.; Ania, C. O.; Doblaré, M.; Calero, S. Insights on the Molecular Mechanisms of Hydrogen Adsorption in Zeolites. *J. Phys. Chem. C* **2013**, *117*, 14374−14380.

(53) van den Berg, A. W.; Bromley, S. T.; Wojdel, J. C.; Jansen, J. C. Adsorption isotherms of H_2 in microporous materials with the SOD

(54) Pantatosaki, E.; Papadopoulos, G. K. On the computation of long-range interactions in fluids under confinement: Application to pore systems with various types of spatial periodicity. *J. Chem. Phys.* **2007**, *127*, No. 164723.

(55) Garberoglio, G.; Skoulidas, A. I.; Johnson, J. K. Adsorption of Gases in Metal Organic Materials: Comparison of Simulations and Experiments. *J. Phys. Chem. B* **2005**, *109*, 13094−13103.

(56) Martin-Calvo, A.; Gutiérrez-Sevillano, J. J.; Matito-Martos, I.; Vlugt, T.J.H.; Calero, S. Identifying Zeolite Topologies for Storage and Release of Hydrogen. *J. Phys. Chem. C* **2018**, *122*, 12485−12493.

(57) O'Keeffe, M.; Peskov, M. A.; Ramsden, S. J.; Yaghi, O. M. The Reticular Chemistry Structure Resource (RCSR) Database of, and Symbols for, Crystal Nets. *Acc. Chem. Res.* **2008**, *41*, 1782−1789.

(58) Eddaoudi, M.; Sava, D. F.; Eubank, J. F.; Adil, K.; Guillerm, V. Zeolite-like metal−organic frameworks (ZMOFs): design, synthesis, and properties. *Chem. Soc. Rev.* **2015**, *44*, 228−249.

(59) Aguado, S.; Bergeret, G.; Titus, M. P.; Moizan, V.; Nieto-Draghi, C.; Bats, N.; Farrusseng, D. Guest-induced gate-opening of a zeolite imidazolate framework. *New J. Chem.* **2011**, *35*, 546−550.

(60) Sánchez-Laínez, J.; Veiga, A.; Zornoza, B.; Balestra, S.R.G.; Hamad, S.; Ruiz-Salvador, A. R.; Calero, S.; Téllez, C.; Coronas, J. Tuning the separation properties of zeolitic imidazolate framework core−shell structures via post-synthetic modification. *J. Mater. Chem. A* **2017**, *5*, 25601−25608.

(61) Houndonougbo, Y.; Signer, C.; He, N.; Morris, W.; Furukawa, H.; Ray, K. G.; Olmsted, D. L.; Asta, M.; Laird, B. B.; Yaghi, O. M. A Combined Experimental−Computational Investigation of Methane Adsorption and Selectivity in a Series of Isoreticular Zeolitic Imidazolate Frameworks. *J. Phys. Chem. C* **2013**, *117*, 10326−10335.

(62) He, M.; Yao, J.; Liu, Q.; Zhong, Z.; Wang, H. Toluene-assisted synthesis of RHO-type zeolitic imidazolate frameworks: synthesis and formation mechanism of ZIF-11 and ZIF-12. *Dalton Trans.* **2013**, *42*, 16608.

(63) Gelb, L. D.; Gubbins, K. E. Pore Size Distributions in Porous Glasses: A Computer Simulation Study. *Langmuir* **1999**, *15*, 305−308.

(64) Sarkisov, L.; Harrison, A. Computational structure character-isation tools in application to ordered and disordered porous materials. *Mol. Simul.* **2011**, *37*, 1248−1257.

(65) Rappe, A. K.; Casewit, C. J.; Colwell, K. S.; Goddard, W. A.; Skiff, W. M. UFF, a full periodic table force field for molecular mechanics and molecular dynamics simulations. *J. Am. Chem. Soc.* **1992**, *114*, 10024−10035.

(66) Sevillano, J. J. G.; Calero, S.; Ania, C. O.; Parra, J. B.; Kapteijn, F.; Gascon, J.; Hamad, S. Toward a Transferable Set of Charges to Model Zeolitic Imidazolate Frameworks: Combined Experimental−Theoretical Research. *J. Phys. Chem. C* **2013**, *117*, 466−471.

(67) Lee, Y.-R.; Jang, M.-S.; Cho, H.-Y.; Kwon, H.-J.; Kim, S.; Ahn, W.-S. ZIF-8: A comparison of synthesis methods. *Chem. Eng. J.* **2015**, *271*, 276−280.

(68) Krokidas, P.; Castier, M.; Moncho, S.; Brothers, E.; Economou, I. G. Molecular Simulation Studies of the Diffusion of Methane, Ethane, Propane, and Propylene in ZIF-8. *J. Phys. Chem. C* **2015**, *119*, 27028−27037.

(69) Pantatosaki, E.; Megariotis, G.; Pusch, A.-K.; Chmelik, C.; Stallmach, F.; Papadopoulos, G. K. On the Impact of Sorbent Mobility on the Sorbed Phase Equilibria and Dynamics: A Study of Methane and Carbon Dioxide within the Zeolite Imidazolate Framework-8. *J. Phys. Chem. C* **2012**, *116*, 201−207.

(70) Zhang, L.; Wu, G.; Jiang, J. Adsorption and Diffusion of CO_2 and CH_4 in Zeolitic Imidazolate Framework-8: Effect of Structural Flexibility. *J. Phys. Chem. C* **2014**, *118*, 8788−8794.

(71) Kim, M. H.; Choi, S.-O.; Choo, S. T. Capability of CO_2 on Metal-Organic Frameworks-Based Porous Adsorbents and Their Challenges to Pressure Swing Adsorption Applications. *Clean Technol.* **2013**, *19*, 370−378.

(72) Rallapalli, P.; Prasanth, K. P.; Patil, D.; Somani, R. S.; Jasra, R. V.; Bajaj, H. C. Sorption studies of CO_2, CH_4, N_2, CO, O_2 and Ar on

structure: A grand canonical Monte Carlo study. *Microporous Mesoporous Mater.* **2006**, *87*, 235−242.

nanoporous aluminum terephthalate [MIL-53(Al)]. *J. Porous Mater.* **2011**, *18*, 205−210.

(73) Klein, R. A.; Shulda, S.; Parilla, P. A.; Le Magueres, P.; Richardson, R. K.; Morris, W.; Brown, C. M.; McGuirk, C. M. Structural resolution and mechanistic insight into hydrogen adsorption in flexible ZIF-7. *Chem. Sci.* **2021**, *12*, 15620−15631.

(74) Noguera-Díaz, A.; Villarroel-Rocha, J.; Ting, V. P.; Bimbo, N.; Sapag, K.; Mays, T. J. Flexible ZIFs: probing guest-induced flexibility with CO_2, N_2 and Ar adsorption. *J. Chem. Technol. Biotechnol.* **2019**, *94*, 3787−3792.

(75) Cuadrado-Collados, C.; Fernández-Català, J.; Fauth, F.; Cheng, Y. Q.; Daemen, L. L.; Ramirez-Cuesta, A. J.; Silvestre-Albero, J. Understanding the breathing phenomena in nano-ZIF-7 upon gas adsorption. *J. Mater. Chem. A* **2017**, *5*, 20938−20946.

(76) Zhou, M.; Wang, Q.; Zhang, L.; Liu, Y.-C.; Kang, Y. Adsorption Sites of Hydrogen in Zeolitic Imidazolate Frameworks. *J. Phys. Chem. B* **2009**, *113*, 11049−11053.

(77) Ma, H.; Wang, Z.; Zhang, X.-F.; Ding, M.; Yao, J. In situ growth of amino-functionalized ZIF-8 on bacterial cellulose foams for enhanced CO_2 adsorption. *Carbohydr. Polym.* **2021**, *270*, No. 118376.

(78) Hwang, J.; Azzan, H.; Pini, R.; Petit, C. H_2, N_2, CO_2, and CH_4 Unary Adsorption Isotherm Measurements at Low and High Pressures on Zeolitic Imidazolate Framework ZIF-8. *J. Chem. Eng. Data* **2022**, *67*, 1674−1686.

(79) Huang, H.; Zhang, W.; Liu, D.; Liu, B.; Chen, G.; Zhong, C. Effect of temperature on gas adsorption and separation in ZIF-8: A combined experimental and molecular simulation study. *Chem. Eng. Sci.* **2011**, *66*, 6297−6305.

(80) Guo, A.; Ban, Y.; Yang, K.; Zhou, Y.; Cao, N.; Zhao, M.; Yang, W. Molecular sieving mixed matrix membranes embodying nanofillers with extremely narrow pore-openings. *J. Membr. Sci.* **2020**, *601*, No. 117880.

(81) Hosseini, S. R.; Omidkhah, M.; Mehri Lighvan, Z.; Norouzbahari, S.; Ghadimi, A. Synthesis, characterization, and gas adsorption performance of an efficient hierarchical ZIF-11@ZIF-8 core−shell metal−organic framework (MOF). *Sep. Purif. Technol.* **2023**, *307*, No. 122679.

(82) Wu, X.; Niknam Shahrak, M.; Yuan, B.; Deng, S. Synthesis and characterization of zeolitic imidazolate framework ZIF-7 for CO_2 and CH_4 separation. *Microporous Mesoporous Mater.* **2014**, *190*, 189−196.

(83) Tagliabue, M.; Farrusseng, D.; Valencia, S.; Aguado, S.; Ravon, U.; Rizzo, C.; Corma, A.; Mirodatos, C. Natural gas treating by selective adsorption: Material science and chemical engineering interplay. *Chem. Eng. J.* **2009**, *155*, 553−566.

(84) Qian, J.; Sun, F.; Qin, L. Hydrothermal synthesis of zeolitic imidazolate framework-67 (ZIF-67) nanocrystals. *Mater. Lett.* **2012**, *82*, 220−223.

(85) Li, J.-R.; Kuppler, R. J.; Zhou, H.-C. Selective gas adsorption and separation in metal−organic frameworks. *Chem. Soc. Rev.* **2009**, *38*, 1477.

(86) Noh, K.; Lee, J.; Kim, J. Compositions and Structures of Zeolitic Imidazolate Frameworks. *Isr. J. Chem.* **2018**, *58*, 1075−1088.

(87) Nguyen, N. T. T.; Furukawa, H.; Gándara, F.; Nguyen, H. T.; Cordova, K. E.; Yaghi, O. M. Selective Capture of Carbon Dioxide under Humid Conditions by Hydrophobic Chabazite-Type Zeolitic Imidazolate Frameworks. *Angew. Chem.* **2014**, *126*, 10821−10824.

(88) Sirjoosingh, A.; Alavi, S.; Woo, T. K. Grand-Canonical Monte Carlo and Molecular-Dynamics Simulations of Carbon-Dioxide and Carbon-Monoxide Adsorption in Zeolitic Imidazolate Framework Materials. *J. Phys. Chem. C* **2010**, *114*, 2171−2178.